International Journal of Advanced Culture Technology Vol.10 No.3 295-306 (2022)
DOI https://doi.org/10.17703/IJACT.2022.10.3.295

IJACT 22-9-35

Numerical Analysis of Flow Uniformity in Selective Catalytic Reduction (SCR) Process Using Computational Fluid Dynamics (CFD)

[1]Byung-Hyun, Shon

[1]Professor, Dept. of Environmental Engineering, Hanseo University, 46, Hanseo 1-ro, Haemi-Myun, Seosan-Si, Chungcheongnam-do, Republic of Korea
bhshon@hanseo.ac.kr

Abstract

The NOx removal performance of the SCR process depends on various factors such as catalytic factors (catalyst composition, shape, space velocity, etc.), temperature and flow rate distribution of the exhaust gas. Among them, the uniformity of the flow flowing into the catalyst bed plays the most important role. In this study, the flow characteristics in the SCR reactor in the design stage were simulated using a three-dimensional numerical analysis technique to confirm the uniformity of the airflow. Due to the limitation of the installation space, the shape of the inlet duct was compared with the two types of inlet duct shape because there were many curved sections of the inlet duct and the duct size margin was not large. The effect of inlet duct shape, guide vane or mixer installation, and venturi shape change on SCR reactor internal flow, airflow uniformity, and space utilization rate of ammonia concentration were studied. It was found that the uniformity of the airflow reaching the catalyst layer was greatly improved when an inlet duct with a shape that could suppress drift was applied and guide vanes were installed in the curved part of the inlet duct to properly distribute the process gas. In addition, the space utilization rate was greatly improved when the duct at the rear of the nozzle was applied as a venturi type rather than a mixer for uniform distribution of ammonia gas.

Keywords: *Ammonia(NH_3), Computational Fluid Dynamics (CFD), Flow uniformity, Nitrogen oxides (NOx), Selective Catalytic Reduction (SCR)*

1. INTRODUCTION

Nitrogen oxides (NO_x), one of the major pollutants in the atmosphere, can theoretically exist in the form of N_2O, NO, NO_2, N_2O_3, N_2O_4, NO_3 and N_2O_5. However, NOx in exhaust gases typically consists of >95% NO and <5% NO_2, which can vary slightly with temperature and atmosphere (especially for the concentrations O_2 and CO) [1]. The selective catalytic reduction (SCR) for NO_x using NH_3 as a reductant is a technology introduced in the late 1970s. This is one of the widely used technologies for reducing NO_x in flue gas generated from coal-fired power plants and other industrial facilities [2]. The SCR method is the most widely used nitrogen oxide treatment technology in the world and is currently applied in more than 500 commercialized processes [3,4]. NO_x in flue gases can be converted to N_2 and H_2O using a catalyst in the presence of oxygen. Reducing agents used in the SCR process include ammonia, urea, and hydrocarbons. Among them, the SCR

Manuscript received: July 14, 2022 / revised: August 16, 2022 / accepted: September 01, 2022
Corresponding Author: bhshon@hanseo.ac.kr
Tel: +82-41-660-1368, Fax: +82-41-660-1368
Professor, Dept. of Environmental Engineering, Hanseo Univ., Korea

process using NH_3 is relatively reliable than the process using other reductants, and the reaction formula is as follows [3,5].

$$4NH_3 + 4NO + O_2 \rightarrow 4N_2 + 6H_2O \quad (1)$$
$$4NH_3 + 2NO_2 + O_2 \rightarrow 3N_2 + 6H_2O \quad (2)$$
$$2NH_3 + NO + NO_2 + O_2 \rightarrow 2N_2 + 3H_2O \quad (3)$$

SCR method is used for more than 90% of NO_x treatment of exhaust gas from thermal power plants [6,7]. However, since SCR has a narrow operating temperature range (300-400°C.), large amount of catalyst is required to increase reaction efficiency and the temperature of exhaust gas must be lowered. Ammonia slip and equipment corrosion, catalyst life, etc. are also important issues with SCR. In general, most of the spent catalyst had used in SCR is recycled or reused, but if not recycled, the spent catalyst must be treated in a sanitary landfill [8].

In NO_x emissions can be controlled in three different ways: pre-combustion, combustion control and post-combustion. Using pre-combustion and combustion methods, NO_x can be reduced to less than 50%. The pre-combustion method is to reduce the amount of nitrogen compounds in the fuel to reduce NOx emissions. Combustion control is to control the temperature of the furnace and burner, control the residence time of the combustion zone, and optimize the air-to-fuel ratio to minimize NO_x production [9]. The post-combustion method is to remove NOx from the exhaust gas emitted after pre-combustion and combustion control.

NO_x during fuel combustion can be classified into Thermal-NO_x, Prompt-NO_x and Fuel-NO_x according to its formation mechanism. Thermal-NO_x is produced by oxidation of N_2 in air under high temperature conditions (>,1450ºC). Therefore, thermal NO_x is generated at very high temperatures and is proportional to the gas residence time and O_2 concentration in the high temperature region [10]. Prompt-NO_x is produced by the reaction between N_2 and hydrocarbon radicals (eg. CH, C_2H and CH_2) in fuel-rich zones. Fuel-NO_x is produced by oxidation of nitrogenous species (char-nitrogen and volatile-nitrogen, mainly HCN and NH_3) contained in fuel. In general, the fuel-NO_x mechanism involves the rapid conversion of nitrogen compounds in the fuel to intermediate nitrogen compounds (mainly in terms of HCN, CN, NH_2, NH, N) and then either reacting with oxygen to convert to NO or be converted to N_2 by reaction with NO itself [11].

The efficiency of SCR is affected by many factors such as catalyst type, catalyst location, and ammonia distribution. A perfect distribution of NH_3 is very important to maintain a suitable NH_3/NO_x ratio and to reduce NH_3 slip [12]. The NO_x reduction performance of SCR depends on various factors such as catalytic factors (catalyst components, shape, space velocity, etc.) and flue gas temperature, flow rate distribution, and process operating conditions [13,14]. When the performance of the catalyst is guaranteed, the concentration distribution and uniformity of the flow of ammonia flowing into the catalyst bed become the most important factors for NO_x reduction efficiency. This is because, if the flow is not uniform, drift will occur at the front of the catalyst, and only a certain catalyst will be used, which may reduce the catalyst use cycle and reduce the performance of SCR. For uniform airflow distribution of ammonia delivered to the catalyst bed, it is most preferable that the process gas be introduced directly from the top of the reactor. However, in the actual field, the installation space is narrow, so a rational design is impossible, so it is often designed with a side entry structure. Therefore, for flow uniformity in the SCR, a device capable of changing the flow such as a guide vane or a perforated plate must be installed [15].

In this study, the flow characteristics of the SCR reactor in which the exhaust gas is introduced from the side of the upper part of the reactor due to the limitation of the installation space were simulated using a three-dimensional numerical analysis technique. In addition, we tried to study the effects of guide vanes, baffles, and perforated plates on the flow characteristics of ammonia flowing into the SCR reactor.

2. NUMERICAL ANALYSIS AND EXPERIMENT

2.1 Basic equation

2.1.1 Continuity equation

It is based on the equation of conservation of mass, which means that the mass increase in the control volume is equal to the amount of mass entering through the control volume, and it is given in Eq. (4) [16].

$$\frac{\partial(\rho u_i)}{\partial x_i} = 0 \tag{4}$$

2.1.2 Momentum equation

The momentum equation means that the sum of the forces acting on the control volume is equal to the change in the momentum all of the control volume, as shown in Eq. (5) [16]. In Eq. (5), each term represents the momentum that flows perpendicular to each direction of the control volume, the pressure acting on the control volume, and the gravity due to the difference in density and viscous force acting on the control volume.

$$\frac{\partial(\rho u_i u_j)}{\partial x_j} = -\frac{\partial p}{\partial x_i} + \frac{\partial}{\partial x_j}\left[\mu\left(\frac{\partial u_i}{\partial x_j} + \frac{\partial u_j}{\partial x_i}\right)\right] + \rho g_i \tag{5}$$

2.1.3 Energy equation

The rate of change of energy in the control volume can be obtained from the first law of thermodynamics, which states that it is equal to the sum of the rate of change of work and heat applied to the control volume, and it is expressed in Eq. (6) [16]. This energy equation is used to predict thermal shear phenomena and temperature distribution.

$$\frac{\partial}{\partial x_i}(\rho u_j k) = \frac{\partial}{\partial x_i}\left[\left(\frac{\mu}{\mathrm{Pr}} + \frac{\mu_t}{\mathrm{Pr}t}\right)\frac{\partial T}{\partial x_i}\right] + S_T \tag{6}$$

2.1.4 Turbulence model

The flow of turbulence is very irregular and shows abnormal three-dimensional behavior, therefore turbulence model is introduced [16]. In the turbulence model, turbulence movement is largely expressed in two properties: First, velocity scale to represent intensity of turbulence and second, length scale to represent size of turbulence. Among turbulence models, the k-ε model proposed by Launder and Spalding in 1974 [17], which is a modification of Navier-Stokes Eq. (7), is best model to express turbulence. Standard k-ε turbulence model expresses turbulence viscosity in turbulence kinetic energy and dissipation rate of turbulence. Equations for turbulence kinetic equation is as follows [16].

$$\frac{\partial}{\partial x_k}(\rho u_k k) = \frac{\partial}{\partial x_k}\left[\left(\mu + \frac{\mu_t}{\sigma_k}\right)\frac{\partial k}{\partial x_k}\right] + \mathrm{P} - \rho\varepsilon \tag{7}$$

Equation for dissipation rate of turbulence is as shown in Eq. (8) where P means the turbulence generation term, as in Eq. (9) [16].

$$\frac{\partial}{\partial x_k}(\rho u_k \varepsilon) = \frac{\partial}{\partial x_k}\left[\left(\mu + \frac{\mu_t}{\sigma_k}\right)\frac{\partial \varepsilon}{\partial x_k}\right] + C_1 \frac{\varepsilon}{k} P - C_2 \frac{\rho \varepsilon^2}{k} \quad (8)$$

$$P = -\rho u_i u_k \frac{\partial u_i}{\partial x_k} = \mu_t \left(\frac{\partial u_i}{\partial x_k} + \frac{\partial u_k}{\partial x_i}\right)\frac{\partial u_i}{\partial x_k} \quad (9)$$

And the turbulent viscosity coefficient μ_t can be expressed as the relation between the turbulent kinetic energy k and the energy dissipation rate ε as shown in Eq. (10). This turbulence model can only be used in the complete turbulence region and uses a wall function in the vicinity of the wall. The constants used in this turbulence model are 1.44 for C_1, 1.92 for C_2, 0.09 for C_μ, and 1.3 for σ_k, respectively [16].

$$\mu_t = C_\mu \rho \frac{K^2}{\varepsilon} \quad (10)$$

2.2 Porous media model

Since it is difficult to implement complex shapes such as catalysts with current computational fluid technology, a porous media model is used to assume a porous material and calculate the pressure drop per unit length for the local flow rate [18]. Ignoring convective acceleration and diffusion, the porous media model is reduced to Darcy's Law;

$$\nabla P = -\frac{\mu}{\alpha}\vec{v} \quad (11)$$

The pressure drop in each of the three coordinate directions (x, y, z) in a porous region is given by Eqs. (12)-(14).

$$\Delta p_x = \sum_{j=1}^{3} \frac{\mu}{\alpha_{xj}} v_j \, \Delta n_x \quad (12)$$

$$\Delta p_y = \sum_{j=1}^{3} \frac{\mu}{\alpha_{yj}} v_j \, \Delta n_y \quad (13)$$

$$\Delta p_z = \sum_{j=1}^{3} \frac{\mu}{\alpha_{zj}} v_j \, \Delta n_z \quad (14)$$

2.3 Condition for numerical analysis

Many A commercial software FLUENT was used and the turbulence equation is discretized by finite volume method. All numerical analysis was performed using upwind differencing scheme. In which, artificial diffusion, that is, numerical diffusion was introduced for the convection term, which provides a stable solution. Then, Semi-Implicit Method Pressure-Linked Equations algorithm combining continuity equation and momentum equation was used to find pressure field [4]. Also, under relaxation method was used to improve the convergence. As the basic equation required for numerical analysis is non-linear, convergence of solution by repetition is necessary. During the repetitive calculations, residual (R) was checked to evaluate the convergence of dependent variables, and when the residual reached below 10-3, it was assumed to be converged [19].

$$\max \mid \varphi^{n+1} - \varphi^{n} \mid \ \leq 10^{-3} \quad (15)$$

2.4 Analytical model and boundary conditions

The simulation was performed over three steps. In the first simulation, two duct lay-outs were proposed to select a suitable duct layout for the factory where this SCR facility will be installed, and then the airflow flow and flow velocity distribution inside the duct were compared.

3. RESULTS AND DISCUSSION

3.1 1st simulation model

In the first simulation, two duct lay-outs were proposed to select a suitable duct layout as can be seen in Fig. 1. As detailed in Fig. 1, 16.3 kg/hr (9% NH_4OH, 20°C) of ammonia water was injected using a spray nozzle for ammonia injection (spray angle 20°, air flow rate of 10.8 Nm^3/hr), and the exhaust gas flow rate was 48,159 m^3/hr at 170 °C.

Simulation model		Simulation conditions
Case-1	Case-2	
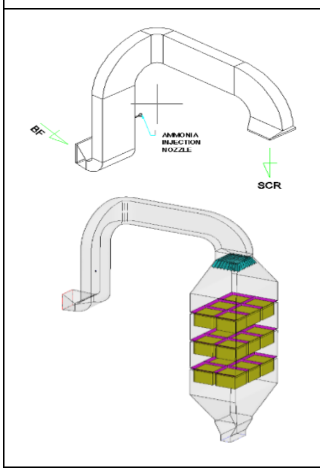	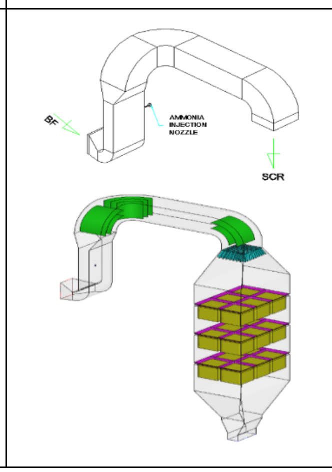	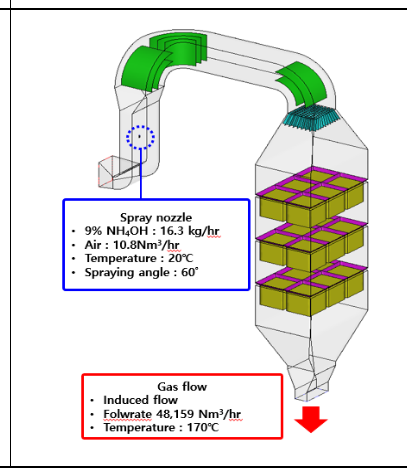

Figure 1. Boundary conditions for 1st simulation model

3.1.1 Air flow distribution

Case-1	Case-2
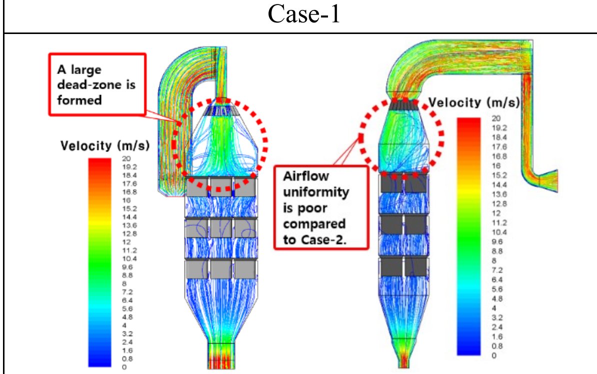	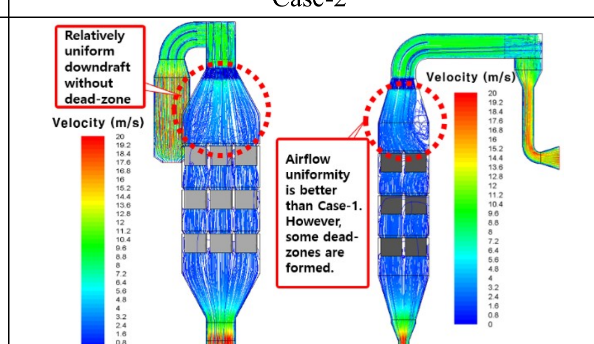

Figure 2. Air flow distribution in the 1st simulation

Fig. 2 shows the simulation results for the air flow distribution passing through the catalytic bed as well as the inlet of the catalyst bed. As shown in Fig. 2, it can be seen that in Case-1, a severe dead-zone occurs at the inlet of the catalyst layer and there is a large air flow difference between the center of the catalyst layer and the wall. However, in Case-2, it can be seen that the dead-zone at the inlet of the catalyst layer is much improved than in Case-1, and the air flow deviation inside the catalyst layer is also reduced.

3.1.2 Catalytic bed flow velocity distribution

Fig. 3 shows the flow velocity distribution through the cross section of the catalytic bed. The total catalyst bed is divided into three layers, and one layer consists of 6 cells. In Case-1, it can be seen that the flow velocity passing through the six cells of the upper catalyst layer varies greatly from 2.8 m/s to 6.8 m/s. However, in Case-2, the flow velocity passing through the six cells of the upper catalyst layer was 2.2 m/s to 3.5 m/s, indicating that the flow velocity deviation was smaller than in Case-1.

	Cross-sectional distribution	Velocity plotting
Case-1	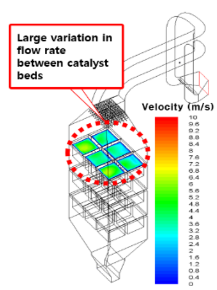	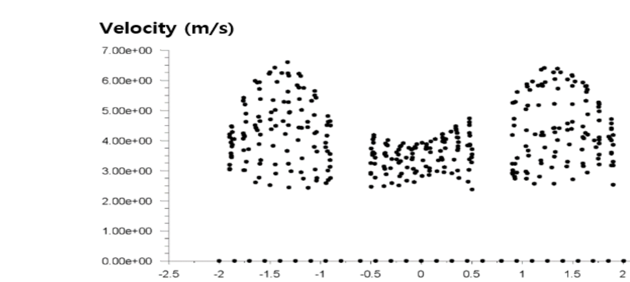
Case-2	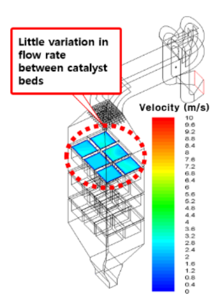	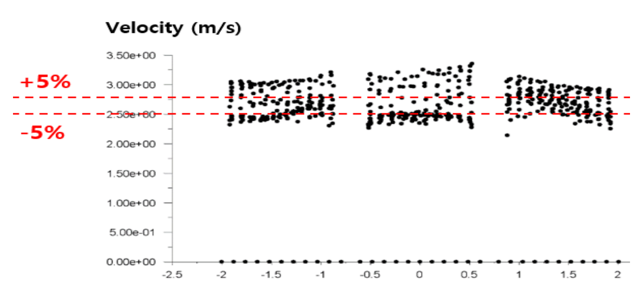

Figure 3. Catalytic bed flow velocity distribution in the 1st simulation

As a result of simulating the flow rate distribution through the catalyst bed, it was found that the flow rate standard value exceeded ±5% in both cases. In Case-1, the air flow uniformity was poor and the flow velocity deviation was very large compared to Case-2 because the inlet duct was narrow and the inflow speed was fast. Therefore, it is desirable to select Case-2 rather than Case-1 to find a way to reduce the flow velocity deviation.

3.2 2nd simulation model

In the second simulation, various design factors were reviewed so that the optimal SCR performance could occur in the duct shape in the layout 2 selected in the first review. The design factors studied in this simulation are i) addition of guide vane, ii) type of mixer, iii) number and position of nozzles, and iv) shape and position of venturi. And the simulation conditions are the same as the first simulation conditions. As shown in Fig. 4, the simulation was carried out while various design factors were changed (6 cases) so that the duct selected in the first simulation could show the optimum efficiency.

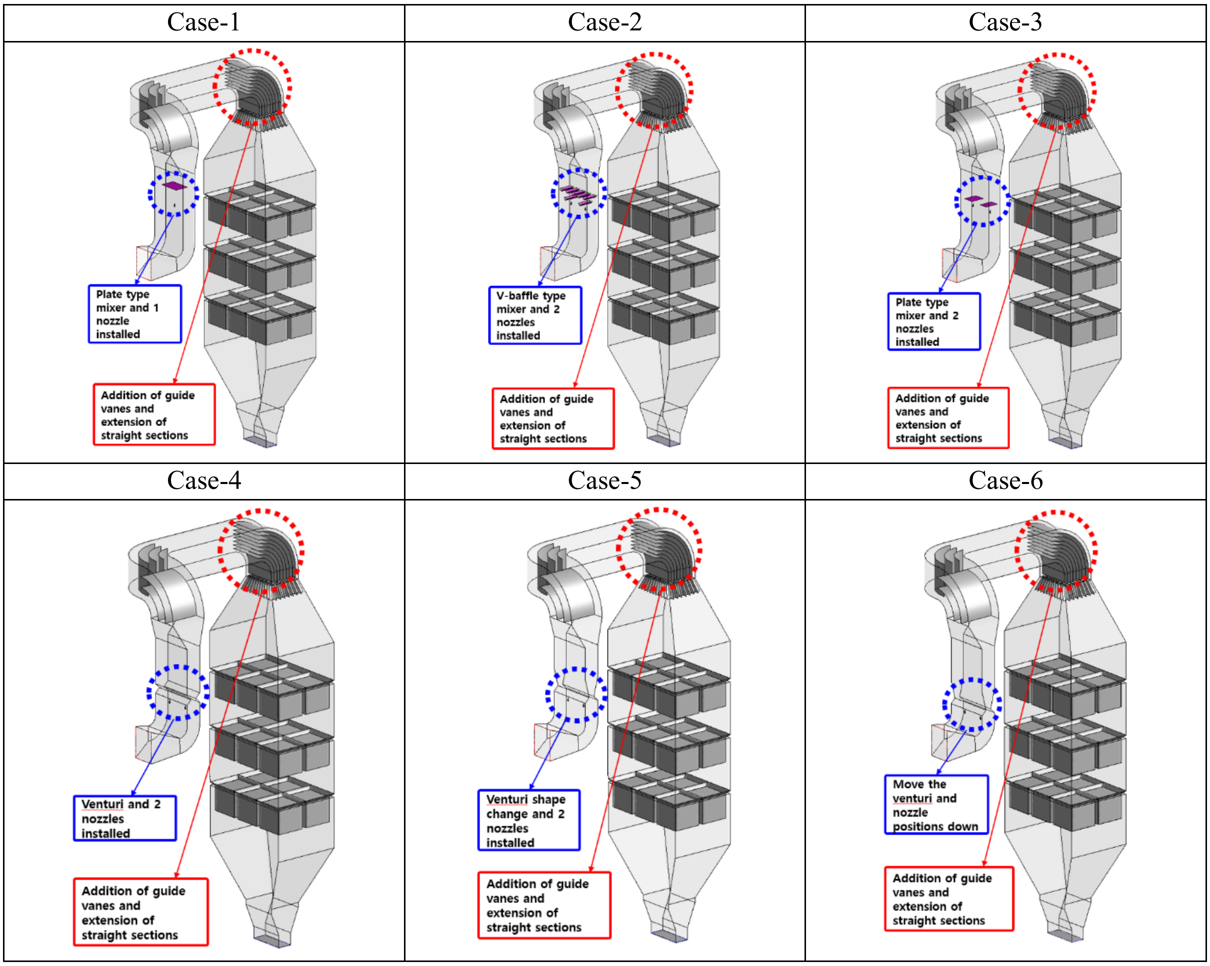

Figure 4. Boundary conditions of the 2rd simulation model

As detailed in Fig. 4, Case-1 adds guide vanes and installs one nozzle and plate-type mixer. In Case-2, a guide vane was added and two nozzles and a V-baffle type mixer were installed. In Case-3, a guide vane is added and two nozzles and a plate-type mixer are installed. In Case-4, a guide vane and two nozzles were installed, and a venturi was installed instead of a plate-type mixer. Case-5 installed a guide vane and two nozzles and changed the shape of the venturi. Finally, Case-6 is the same as Case-5, but the positions of the venturi and nozzle are slightly shifted downwards.

Table 1. Flow and concentration distribution results in the 2nd simulation

	Case-1	Case-2	Case-3	Case-4	Case-5	Case-6
Flow distribution	Excess	Excess	Excess	Excess	Excess	Fitness
Concentration distribution	Excess	Excess	Excess	Excess	Fitness	Fitness
Pressure drop across the reactor (mm H_2O)	158	133	125	150	118	115

In the second simulation, a mixer was installed in the duct selected in the first simulation to understand the effect of the mixer on the improvement of airflow and concentration distribution. As can be seen from Table 1, in case of Case 1~Case 4, both the flow rate and concentration distribution exceeded the standard values, indicating that the mixer effect was insignificant. This seems to adversely affect the airflow uniformity of the catalyst bed because the distance between the mixer and the catalyst bed is too close. In case 5, the concentration standard value was met, but the flow rate distribution was found to exceed the standard value. Installing the venturi is effective in reducing the concentration deviation, but it is considered that the location between the venturi and the catalyst bed is too close, which still adversely affects the airflow uniformity of the catalyst bed. Case 6 was found to meet both the flow rate and concentration distribution standards.

3.3 3rd simulation model

As detailed in Fig. 5, in the 3rd review, the final shape of the reactor in Case 6 selected in the 2nd review was determined, and the flow rate and concentration references of the catalyst bed were checked in detail. In order to improve the catalyst bed flow rate deviation, the guide vanes of the reactor inlet curved part were added and expanded in the duct (layout 2). In addition, to improve the concentration deviation of the catalyst layer, the nozzle position was moved and the duct was configured in a venturi shape.

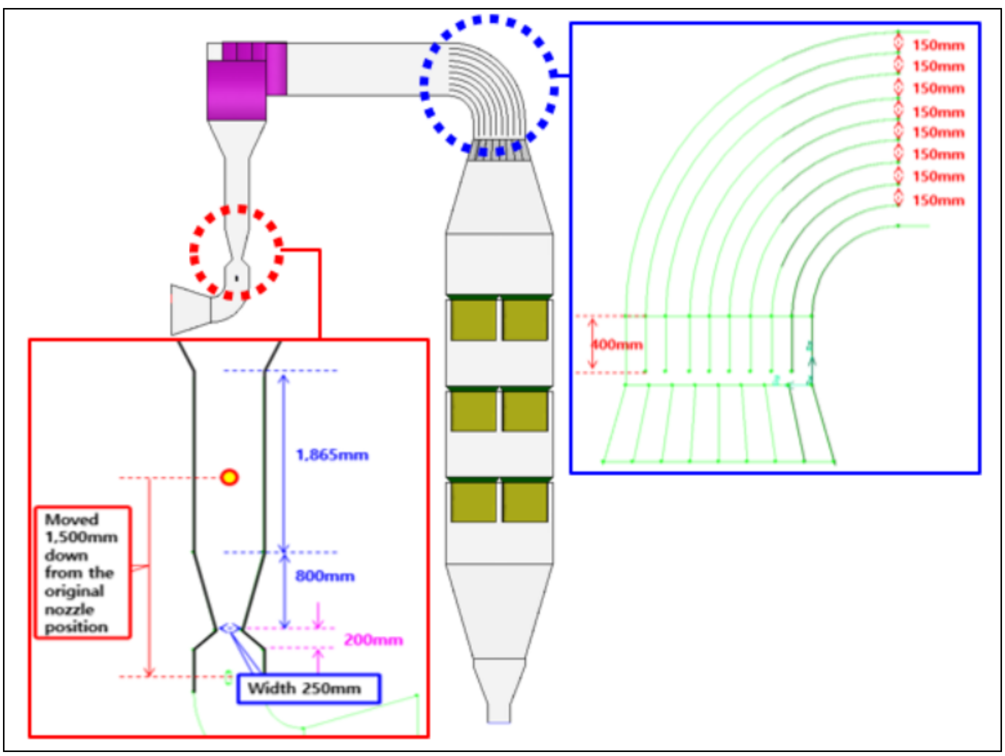

Figure 5. Boundary condition of the 3rd simulation model

3.3.1 Air flow distribution

As shown in Fig. 6, when the shape of Case-6 determined in the secondary simulation is applied, it can be confirmed that the downward airflow is stably formed without the formation of a special vortex on the upper part of the catalyst layer.

3.3.2 NH_3 concentration distribution

As can be seen in Fig. 7, when the shape of Case-6 determined in the secondary simulation is applied, it can be confirmed that the concentration distribution of the airflow flowing into the catalyst layer is uniformly flowing with almost no deviation.

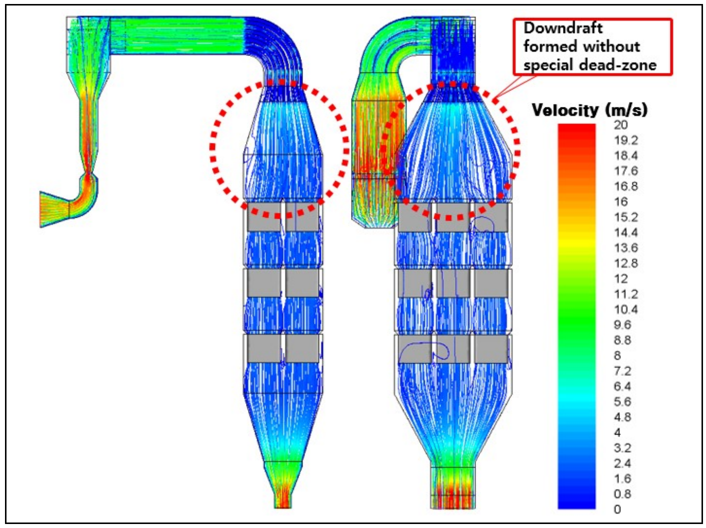

Figure 6. Air flow distribution in 3rd simulation

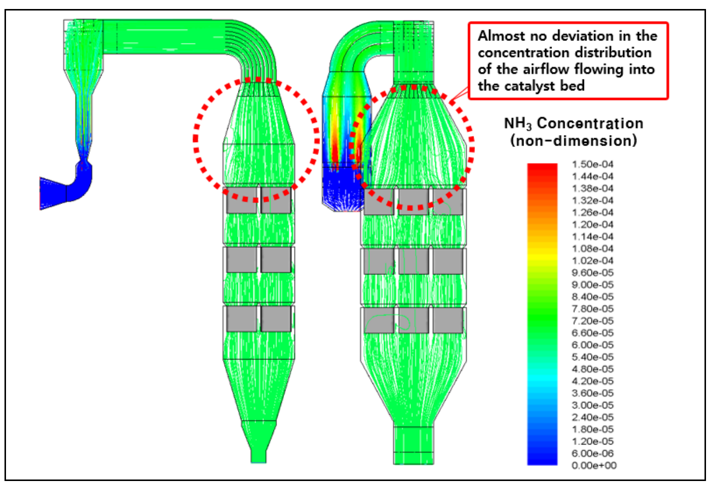

Figure 7. NH_3 concentration distribution in 3rd simulation

3.3.3 Temperature distribution

As can be seen in Fig. 8, when the shape of Case-6 determined in the secondary simulation is applied, it can be confirmed that the temperature distribution of the airflow flowing into the catalyst layer is uniformly flowing with almost no deviation.

3.3.4 Catalytic bed inlet flow velocity and concentration distribution

As can be seen in Fig. 9, it can be confirmed that all flow velocity values flowing through the inlet surface of the catalyst bed are distributed within ±5% of the catalyst performance standard, which satisfies the performance standard.

3.3.5 Pressure distribution

As can be seen in Fig. 10, the differential pressure applied to each stage of the catalyst bed was about 180 Pa, and the total pressure drop of the SCR reactor was confirmed to be 1,152 Pa.

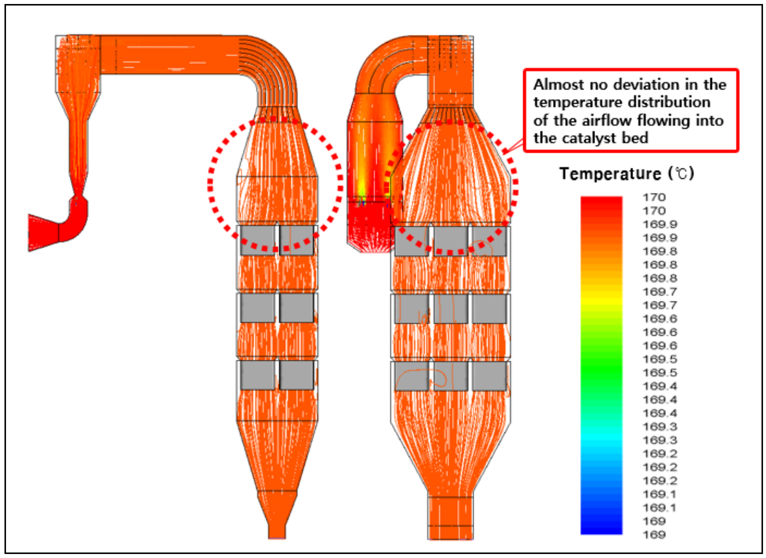

Figure 8. Temperature distribution in 3 rd simulation

Velocity distribution	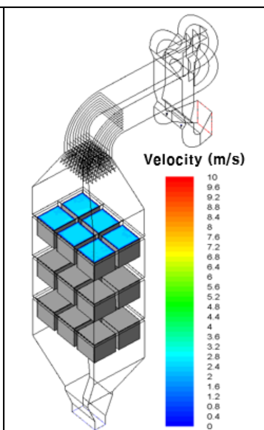	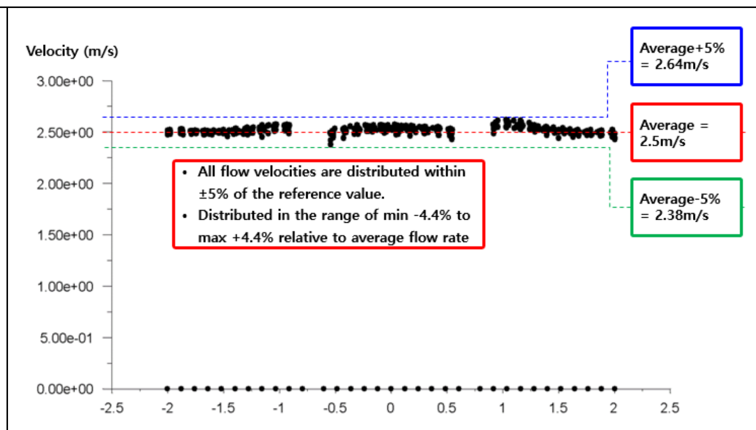
NH_3 concentration distribution	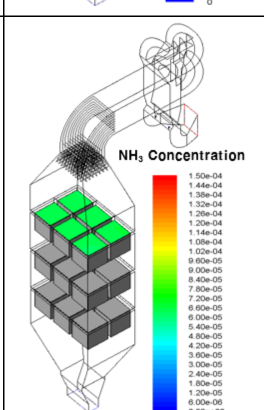	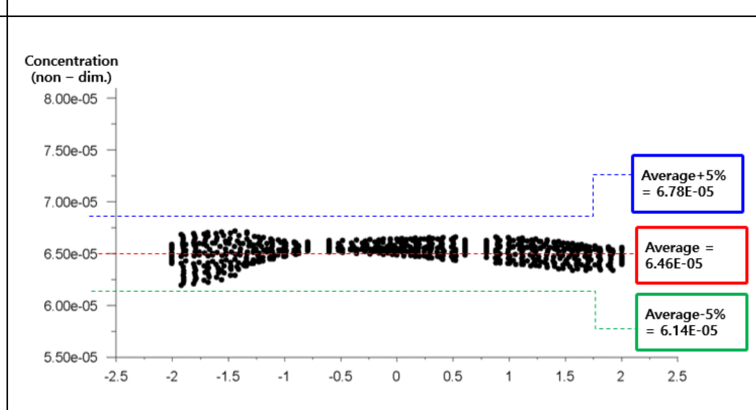

Figure 9. Catalyst bed inlet flow velocity and concentration distribution in 3 rd simulation

In the 3rd simulation, the predicted values of the flow velocity and concentration of the inlet surface of the catalyst layer for the shape of Case-6 were simulated in detail. It was confirmed that they were all distributed within the applicable flow rate and concentration performance standards (deviation ±5%) in the field.

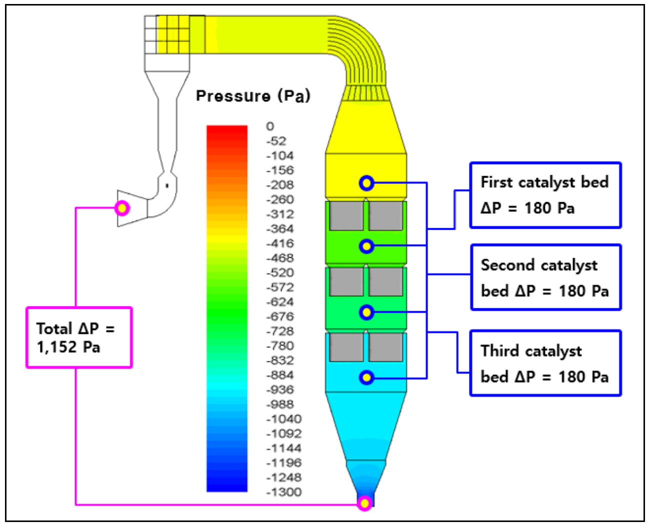

Figure 10. Pressure drop in 3rd simulation

4. CONCLUSION

As a result of studying the factors affecting the NOx removal performance in the SCR process using a three-dimensional numerical analysis technique, the following conclusions were obtained.

Comparing and examining the inlet duct shapes Case-1 and Case-2 in the first review, both Case-1 and Case-2 exceeded the flow rate standard. In Case-1, the width of the inlet duct is narrow and the uniformity of airflow is poor (the inflow velocity is large and the flow velocity deviation is severe), so it is reasonable to apply Case-2. In addition, in order to prepare a plan to solve the flow velocity deviation (guide vane installation, etc.), a secondary simulation was conducted.

Simulating six cases to improve airflow uniformity and ammonia space utilization, the uniformity of airflow reaching the catalyst layer was greatly improved when the exhaust gas was properly distributed by installing a guide vane in the inlet duct curved part. In addition, it was confirmed that the space utilization rate was very good when the duct at the rear end of the nozzle was converted to a venturi type instead of a mixer to improve ammonia distribution.

Analyzing the predicted values of flow velocity and concentration at the inlet surface of the catalyst bed in Case-6, which was finally selected, it was confirmed that all predicted values were distributed within ±5% of the performance standard. In addition, the total pressure drop of the reactor was found to be 1,152 Pa.

ACKNOWLEDGEMENT

This research was supported by the research foundation from Hanseo University in 2020.

REFERENCES

[1] S. Roy, M.S. Hegde, G. Madras, “Catalysis for NOx abatement”, *Appl. Energy*, Vol. 86, No. 11, pp. 2283-2297, 2009.

[2] L. Chen, Z. Si, X. Wu, D. Weng, R. Ran, J. Yu, “Rare earth containing catalysts for selective catalytic reduction of NOx with ammonia: A Review”, *J. Rare Earth*, Vo. 32, pp. 907-917, 2014.

[3] L. Guo, Y. Shu, J. Gao, “Present and future development of flue gas control technology of DeNOx in the World”, *Energy Proc.*, Vol. 17, pp. 397-403, 2012.

[4] H. Park, S. Uhm, "Various technologies for simultaneous removal of NOx and SO2 from flue gas", *Appl. Chem. Eng.*, Vol. 28, pp. 607-618, 2017.
[5] Y. Sun, E. Zwolińska, A.G. Chmielewski, "Abatement technologies for high concentrations of NOx and SO_2 removal from exhaust gases: a review", Crit. Rev. *Environ. Sci. Technol.*, Vol. 46, pp. 119-142, 2016.
[6] G. Cheng, C. Zhang, Desulfurization and denitrification technologies of coal-fired flue gas, *Pol. J. Environ. Stud.*, Vo. 27, 2018.
[7] K. Skalska, J.S. Miller, S. Ledakowicz, Trends in NOx abatement: a review, *Sci. Total Environ.*, Vol. 408, pp. 3976-3989, 2010.
[8] J.L. Sorrels, D.D. Randall, K.S. Schaffner, C.R. Fry, Selective Catalytic Reduction, 2015.
[9] Wojciechowska and Lomnicki, Nitrogen oxides removal by catalytic methods, *Clean Products and Processes*, Vol. 1, pp. 237-247, 1999.
[10] S.K. Hoekman, C. Robbins, Review of the effects of biodiesel on NOx emissions, Fuel Process. Technol. 96 (2012) 237–249, https://doi.org/10.1016/j. fuproc.2011.12.036.
[11] T. Zhang, C. Wu, B. Li, C. Wang, X. Chen, J. Wei, Q. Yu, Clarifying the decomposition process of pyrite and SO_2 release in the cyclone preheater of a dry rotary cement kiln system, *J. Cleaner Prod*. Vol. 241, pp. 118-122, 2019.
[12] Gomez-Garcia MA, Pitchon V, Kiennemann A. Pollution by nitrogen oxides: an approach to NOx abatement by using sorbing catalytic materials. *Environ International*, Vol. 31, pp. 445-467, 2005.
[13] Gang-Woo Lee, Byung-Hyun Shon, Jeong-Gun Yoo, Jong-Hyeon Jung, and Kwang-Joong Oh, "The influence of mixing between NH_3 and NO for a De-NOx reaction in the SNCR process", *Journal of Industrial and Engineering Chemistry*, Vol. 14, No. 4, pp. 457-467, July 2008.
[14] Thanh D.B. Nguyen, Young-Il Lim, Won-Hyeon Eom, Seong-Joon Kim, Kyung-SeunYoo, "Experiment and CFD simulation of hybrid SNCR–SCR using urea solution in a pilot-scale reactor", *Computers & Chemical Engineering*, Vol. 34, No. 10, pp. 1580-1589, 2010.
[15] L.K. Hjertager, B.H. Hjertager, T. Solberg, "CFD modeling of fast chemical reactions in turbulent liquid flows", *Computer Aided Chemical Engineering*, Vol. 9, pp. 159-164, 2001.
[16] Hyun-Guk Myung, Computational Fluid Dynamics for Engineering, Han Mi publishing company, pp. 124-138, 1997.
[17] Patankar SV, Numerical Heat Transfer and Fluid Flow, Hemisphere Publishing Corp., 1980.
[18] Konstantin G. Kornev, Alexander V. Neimark, Aleksey N. Rozhkov, Form in porous media; thermodynamics and hydrodynamic peculiarities, Adnanced in Colloid and Interface Science, Vol. 82, pp. 127-187, 1999.
[19] Witte, J. H., Efficiency and Design of Liquid/Gas Ejector, *British Chemical Engineering*, Vol. 10, No. 9, pp. 602-607, 1995.